Supernovae and Gamma-ray bursts 2014 @RIKEN

Global 3-D simulation of SNRs

- Toward understanding observational features of SNRs

Part II

Masaomi Ono
Department of Physics, Kyushu Univ.
Collaboration with Astrophysical Big-Bang (AAB) Laboratory (RIKEN)

Supernovae to Supernova remnants

Supernova explosions

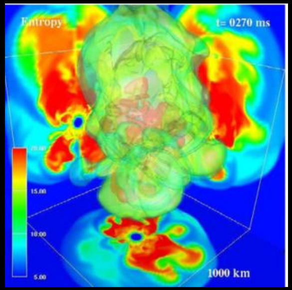

T. Takiwaki

Explosive nucleosynthesis

Mixing

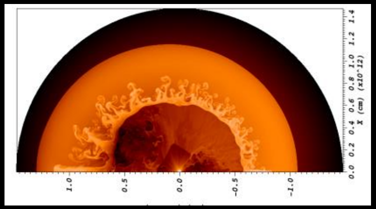

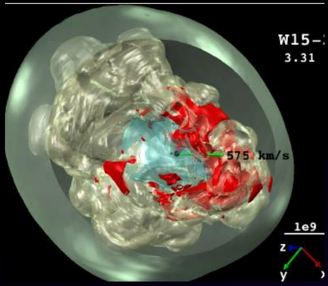

Supernovae

MO and J. Mao

A. Wongwathanarat

Multi-D (MO)

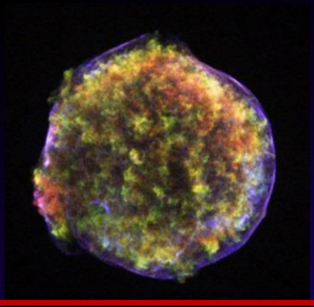

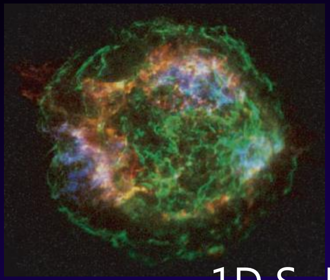

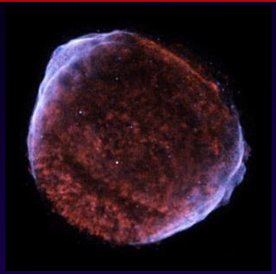

Supernova remnant

1D S.-H., Lee (Herman)

Our final goal

- Make a theoretical model that can be directly compared with observations of SNRs
- Explain observational features of SNRs
- Extract information of the explosion morphology and mechanism

Possible collaboration with members in AAB group members (RIKEN)

S.-H., Lee (Herman)

J. Mao

A. Wongwathanarat

T. Takiwaki

Matter mixing in aspherical core-collapse supernovae - A search for possible conditions for conveying ^{56}Ni into high velocity regions

MO+2013, ApJ, 773, 161

Masaomi Ono[1]

Shigehiro Nagataki[2], Hirotaka Ito[2], Shiu-Hang Lee[2], Jirong Mao[2], Masa-aki Hashimoto[1], Tolstov Alexey[2]

Kyushu University

Astrophysical Big Bang Laboratory, RIKEN

KYUSHU UNIVERSITY

RIKEN

Broadened line profile of [Fe II] in SN 1987A

[Fe II] line profile (Haas et al. 1990)

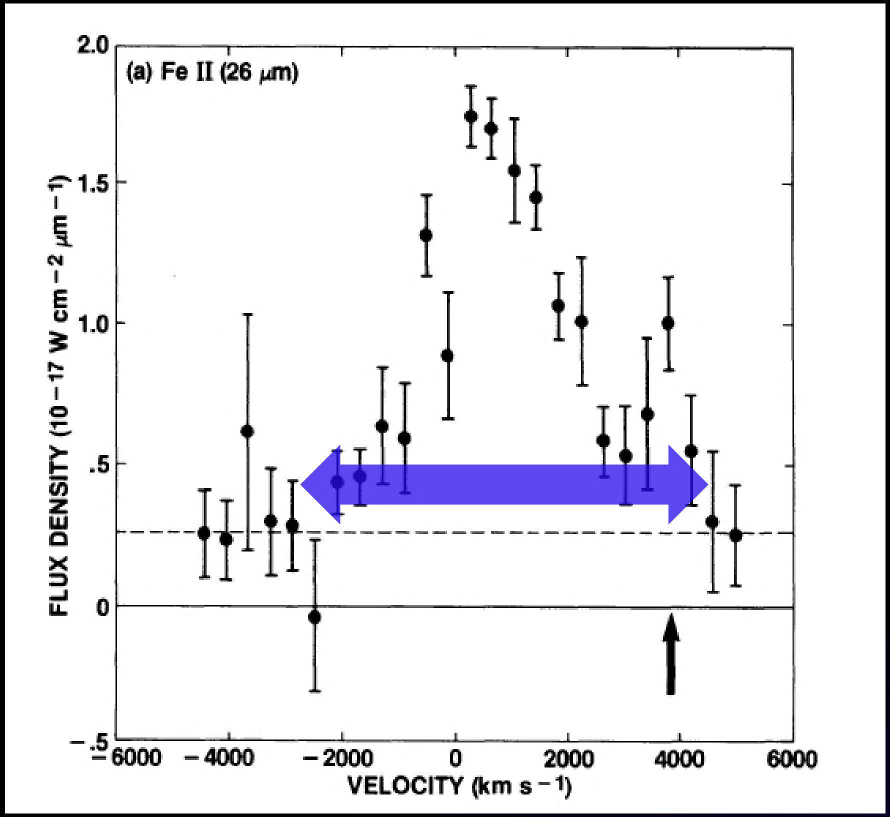

Doppler velocity

4000 km s^{-1}

SN 1987A

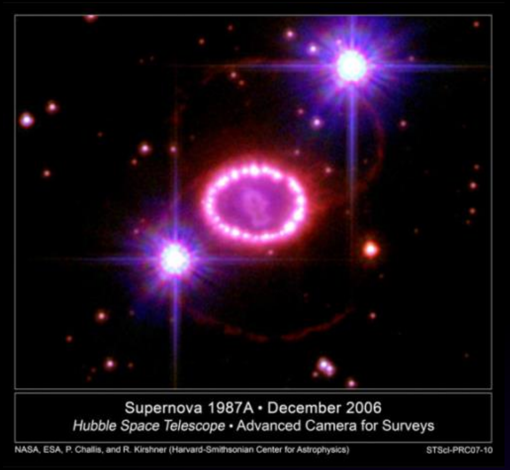

$^{56}Ni \rightarrow {}^{56}Co \rightarrow {}^{56}Fe$

$T_{1/2}$ = 6.1 d $T_{1/2}$ = 77 d

FLASH Code

The FLASH code is a modular, parallel multiphysics simulation code capable of handling general compressible flow problems found in many astrophysical environment (Fryxell et al. 2000)

- Eulerian hydrodynamic code
  - Piecewise Parabolic Method (PPM)
  - Unsplit solver, MHD, RHD
- AMR (Adaptive mesh refinement)
  - Reduce numerical costs
- Many optional units
  - Nuclear reaction networks (7-19 nuclei)

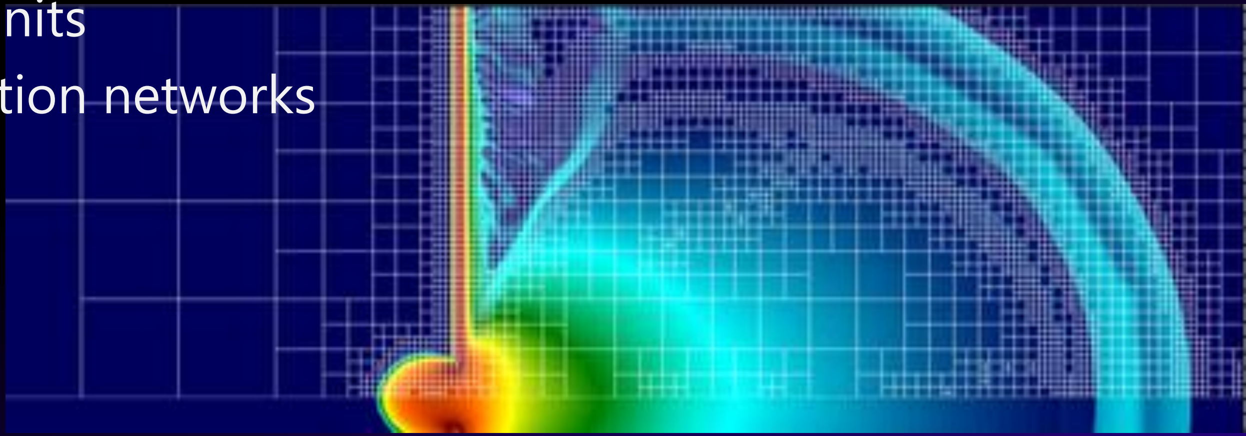

Aspherical explosion with clumpy structure in the explosion (movie)

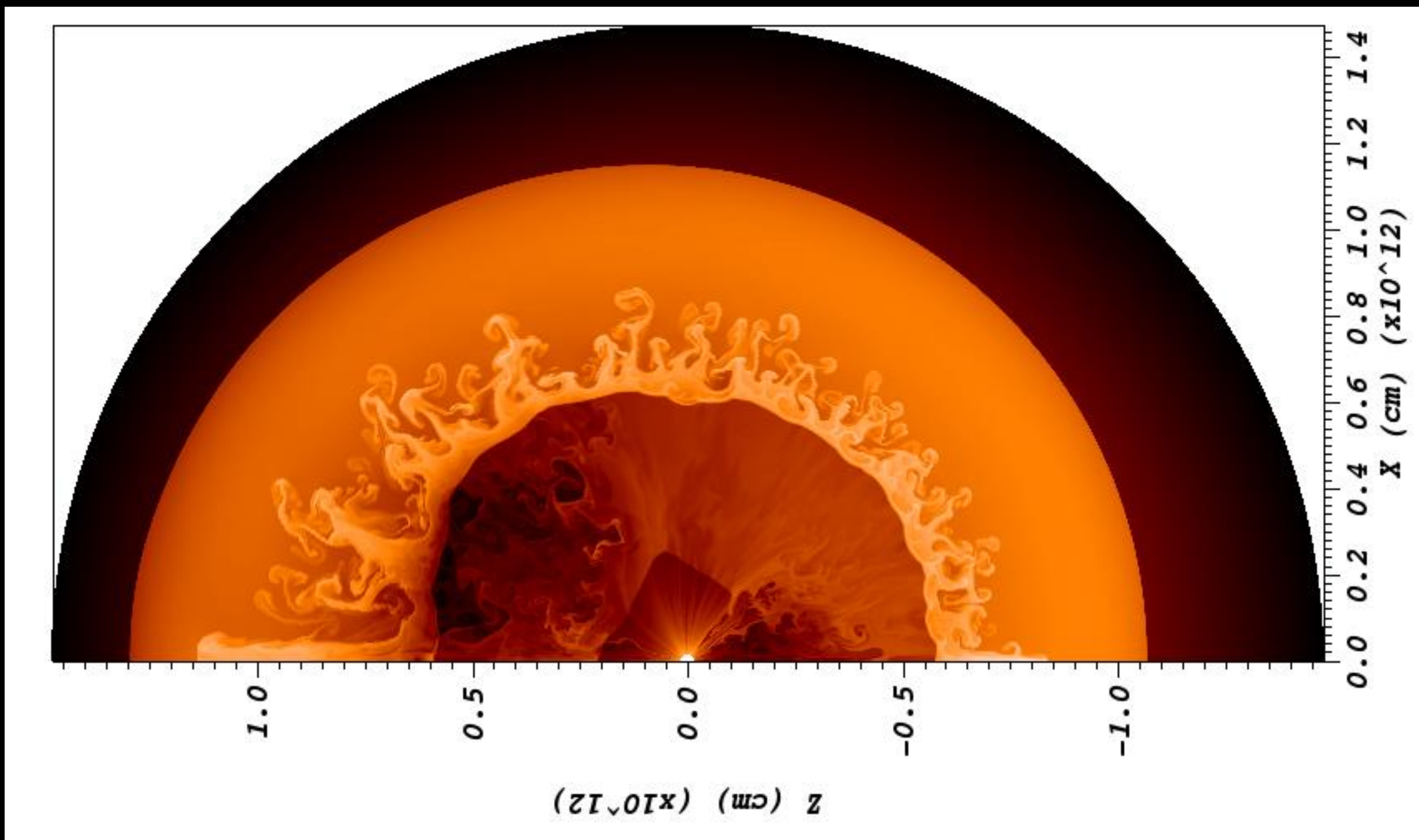

Radial velocity distributions of the best model in this study

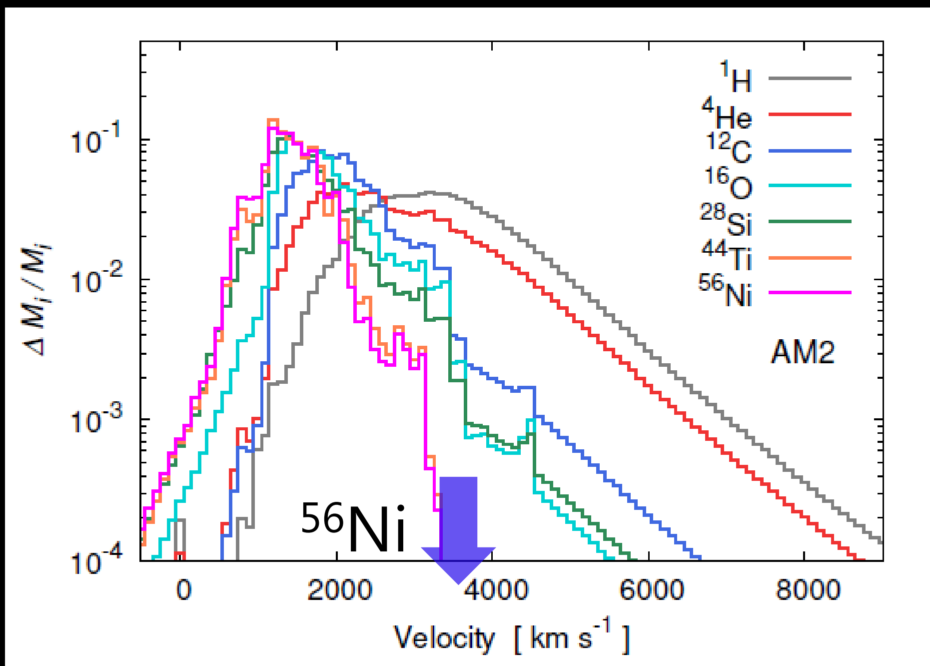

Maximum 3000 km s^{-1}

- Relatively high velocity (3000 km s^{-1}) of ^{56}Ni
- Mass of ^{56}Ni with ~ 3000 km s^{-1} : 1.4 x 10^{-3} $M_\odot$

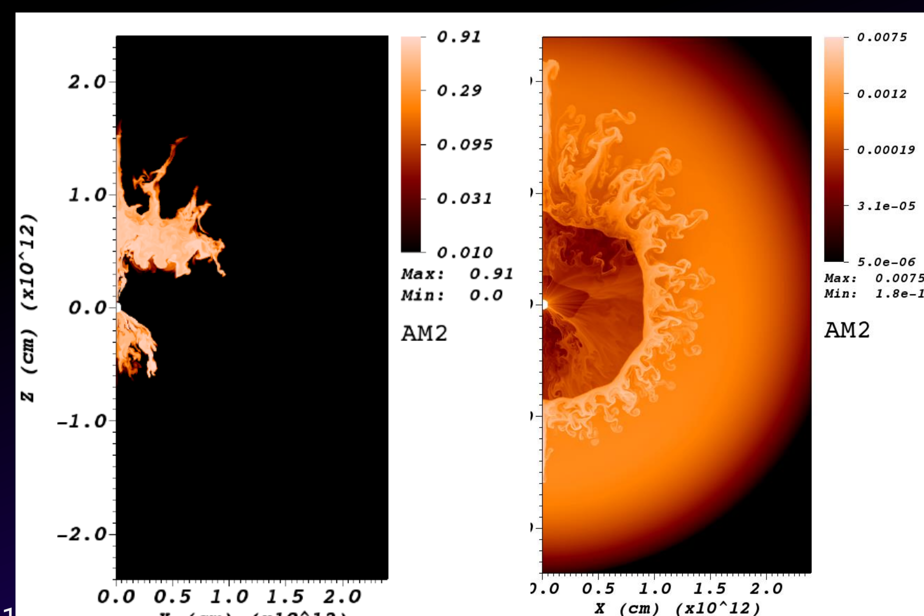

Matter mixing in large density perturbations in the progenitor star

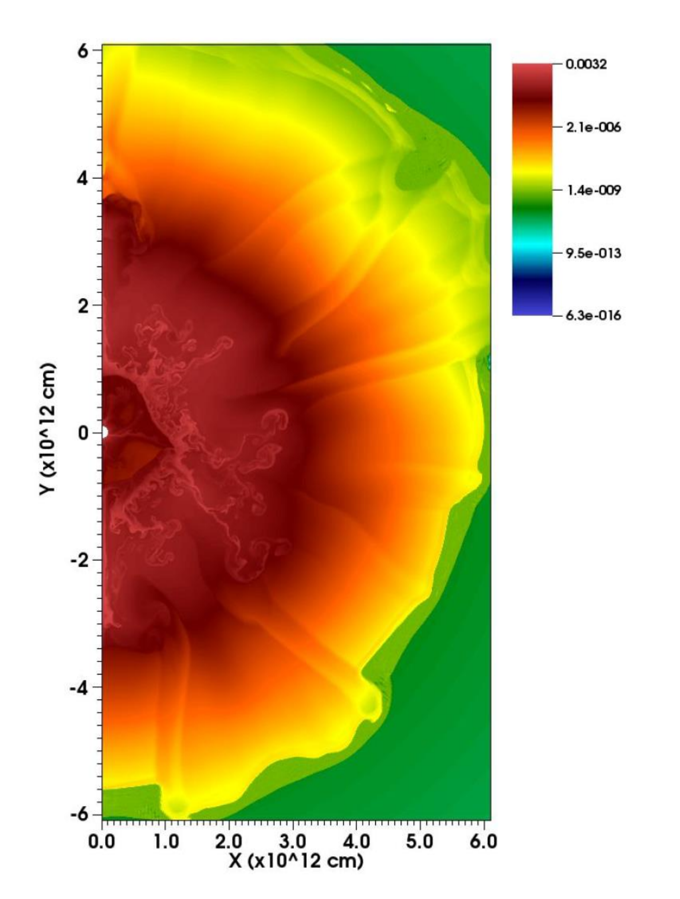

Mao et al. 2014 in prep.

- 2D mixing with large density perturbations

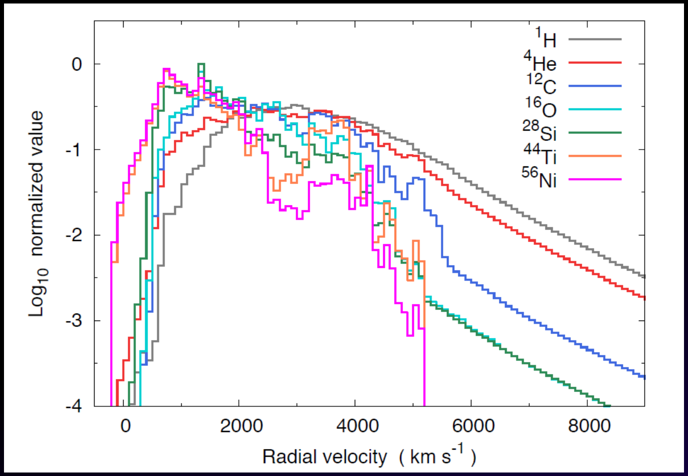

3D structure of Cas A

Delaney et al. 2010

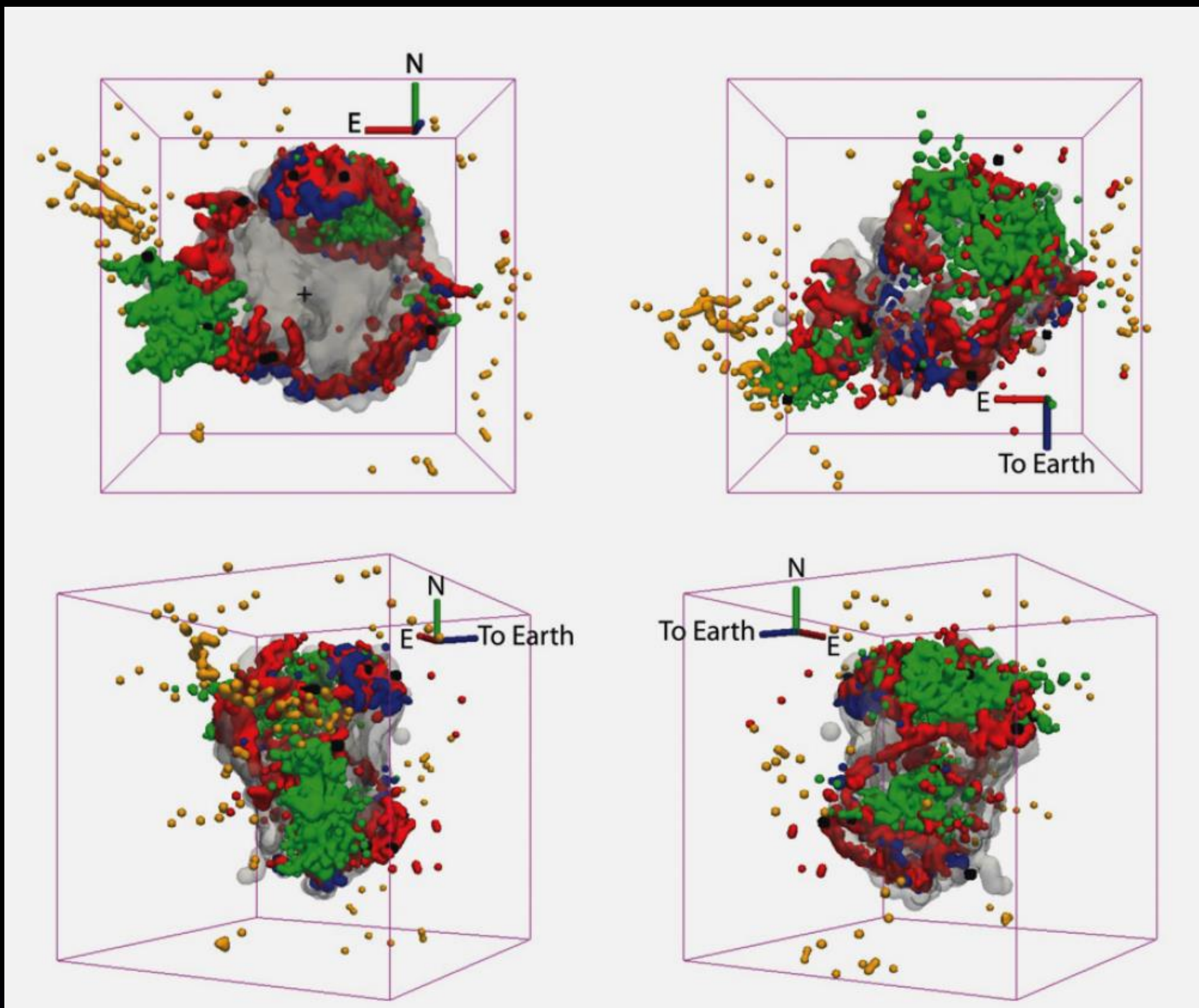

Chandra 's X-rays

Spitzer 's infrared

Green: X-ray Fe-K

Black: X-ray Si XIII

Red: IR [Ar II]

Blue: high [Ne II]/[Ar II] ratio

Grey: IR [Si II]

Yellow: optical outer ejecta

Asymmetries in core-collapse supernovae from maps of radioactive ^{44}Ti in Cas A

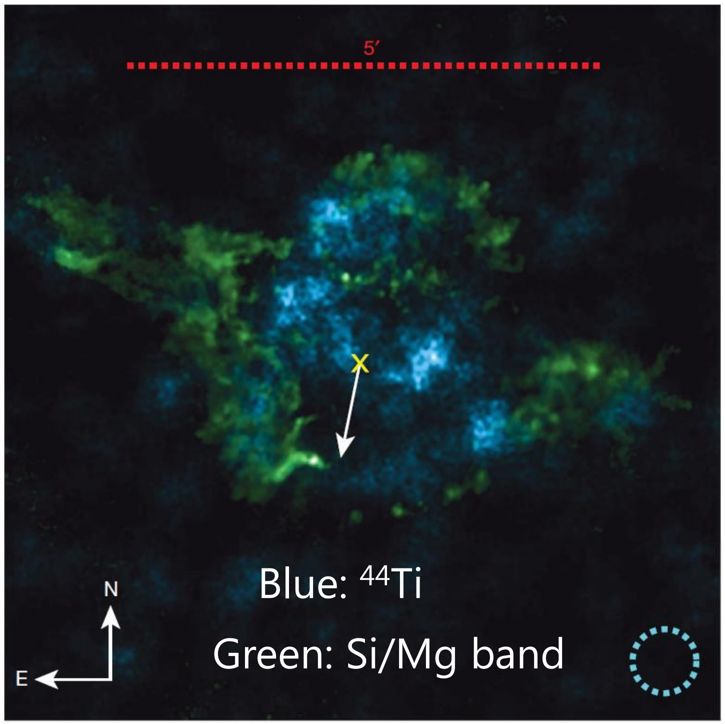

The concentration of Fe-rich ejecta inferred from maps in X-ray atomic transitions is well outside the region where it is synthesized, and not in the centre of the remnant interior to the reverse shock. This observation has been used to suggest the operation of a strong instability similar to that proposed for SN 1993J[23]. The presence of a significant fraction of the ^{44}Ti interior to the reverse shock and the implied presence of interior 'invisible' iron requires this conclusion be revisited.

Figure 2 | A comparison of the spatial distribution of the ^{44}Ti with the known jet structure in Cas A. The image is oriented in standard astronomical coordinates as shown by the compass in the lower left and spans just over 5′ on a side. The ^{44}Ti observed by NuSTAR is shown in blue, where the data have been smoothed using a top-hat function with a radius shown in the lower right (dashed circle). The ^{44}Ti is clearly resolved into distinct knots and is non-uniformly distributed and almost entirely contained within the central 100′′ (Methods and Extended Data Fig. 2). Shown for context in green is the Chandra ratio image of the Si/Mg band (data courtesy of NASA/CXC; Si/Mg ratio image courtesy of J. Vink), which highlights the jet–counterjet structure, the centre of the expansion of the explosion[2] (yellow cross) and the direction of motion of the compact object (white arrow). In contrast to the bipolar feature seen in the spatial distribution of Si ejecta, which argues for fast rotation or a jet-like explosion, the distribution of ^{44}Ti is much less elongated and contains knots of emission away from the jet axis. A reason for this may be that the Si originates in the outer stellar layers and is probably highly influenced by asymmetries in the circumstellar medium, unlike the ^{44}Ti, which is produced in the innermost layers near the collapsing core.

$^{44}Ti \rightarrow {}^{44}Sc \rightarrow {}^{44}Ca$

$T_{1/2}$ = 60 yr $T_{1/2}$ = 4 h

Iron and ^{44}Ti have different distributions

Grefenstette+14, Nature, 506, 339

Cosmic-ray acceleration in SNRs

- Acceleration of cosmic-ray in SNRs
  - Up to 10^{15} eV or more ?
  - Magnetic field is key ingredient

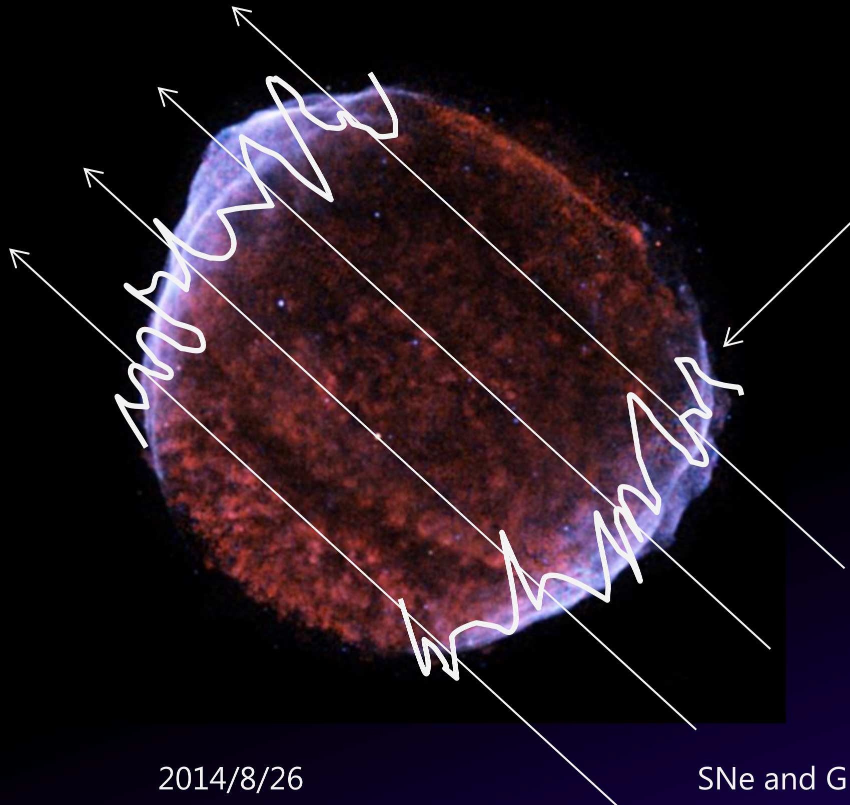

Synchrotron radiation from accelerated electrons

SN1006 (Chandra: X-ray)

Where the acceleration is active?

quasi-perpendicular equatorial belt

e.g., Ellison et al. 1995; Jokipii 1987

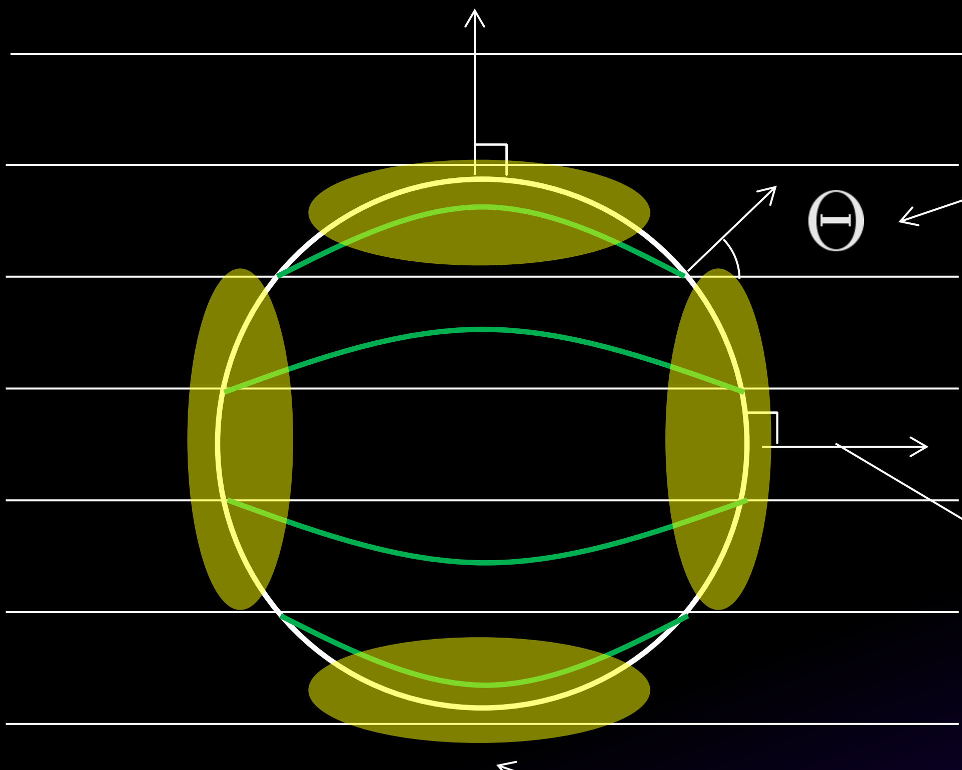

obliquity

Θ

e.g., Rothenflug et al. 2004

quasi-parallel

polar cap

$$\frac{\rho_2}{\rho_1} = \frac{\gamma+1}{\gamma-1} \sim \frac{B_2}{B_1} \to 4 \quad M_1(\to \infty)$$

Radio polarization signature in SN1006

Reynoso et al. 2013, Aston. J, 145, 104

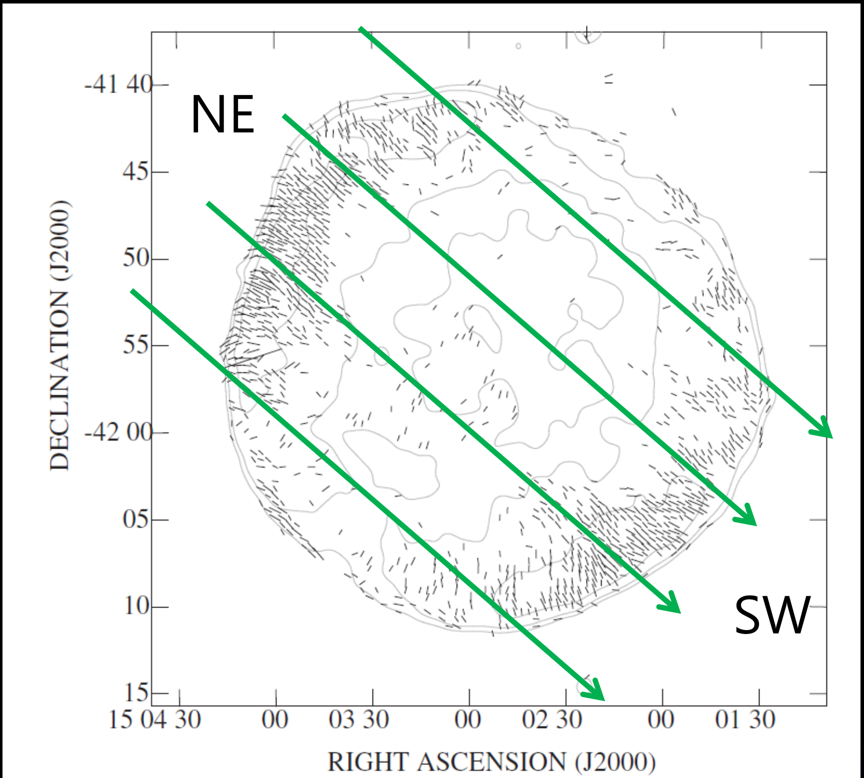

Figure 3. Distribution of magnetic field vectors on SN 1006 at 1.4 GHz corrected for Faraday rotation (assuming uniform RM = 12 rad m^{-2}), at 10 arcsec resolution. Total intensity contours at 10, 20, and 50 mJy $beam^{-1}$ are superposed, where the beam was convolved to 60 arcsec. For the vectors, a length of 30 arcsec represents 0.25 mJy $beam^{-1}$ of polarized flux.

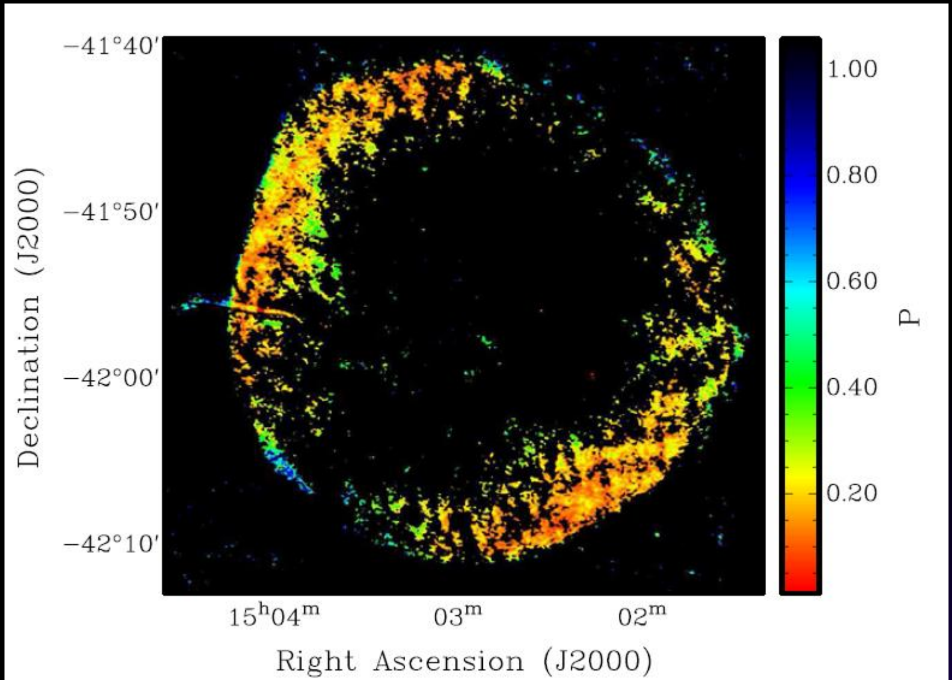

Figure 4. Fractional polarization p of SN 1006 at 1.4 GHz. The resolution is 10 arcsec. The color scale is shown at the right. Only pixels where p was at least twice its error were kept.

Polar cap geometry is favored?

Amplified strong magnetic field ?

Uchiyama et al. 2007, Nature, 4469 576

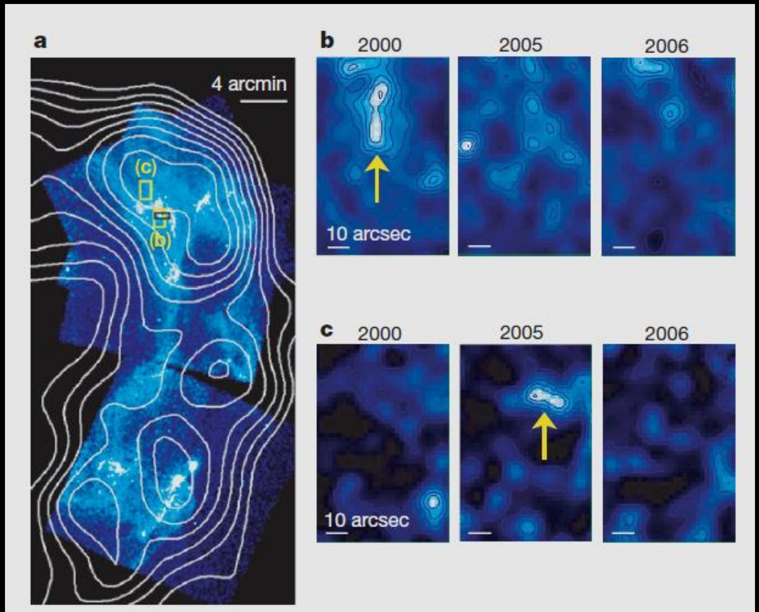

Figure 1 | Chandra X-ray images of the western shell of SNR RX J1713.7−3946. **a**, A Chandra X-ray mosaic image is overlaid with TeV γ-ray contours from HESS measurements[26]. North is up and east is to the

Variations of X-ray hot spots on a 1 yr timescale

Strong amplified magnetic field (～ 100 μ G)?

Bohm-diffusion limit

$$t_{\rm synch} \approx 1.5\,(B/{\rm mG})^{-1.5}\,(\epsilon/{\rm keV})^{-0.5}\,{\rm yr} \qquad \eta \approx 1$$

$$t_{\rm acc} \approx 1\,\eta\,(\epsilon/{\rm keV})^{0.5}\,(B/{\rm mG})^{-1.5}\,(v_{\rm s}/3,000\,{\rm km\,s^{-1}})^{-2}\,{\rm yr}$$

Amplification of b-field and particle acceleration

- What is the mechanism of the amplification of magnetic field?
  - Matsumoto-san's talk
  - RT instability ?

- Where the acceleration is active?
  - quasi-parallel
  - quasi-perpendicular

3D simulation of a Type Ia SNR

Warren and Blondin 2013

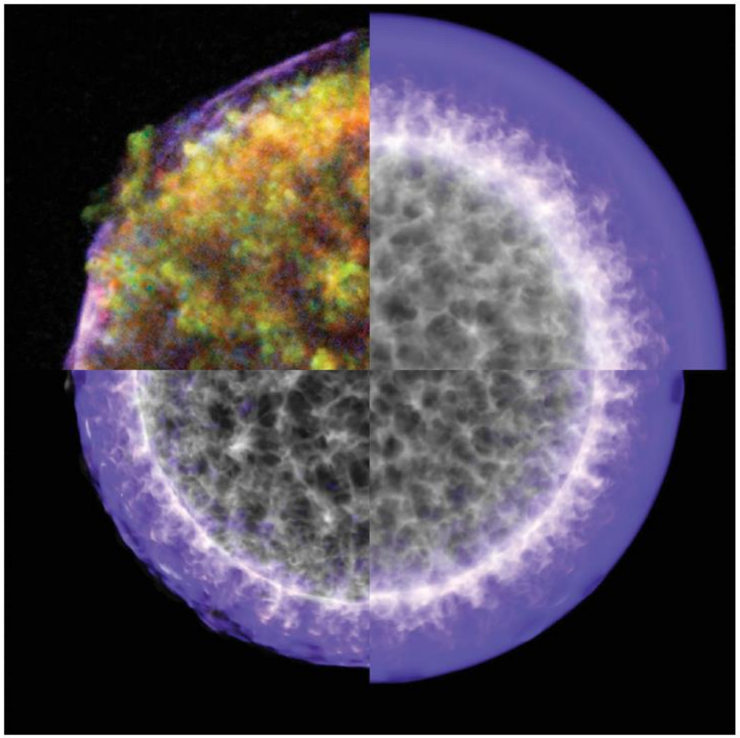

Figure 9. Images showing the effect that changing the adiabatic index γ of the simulation has on the resultant remnant. The SW quadrant of Tycho's SNR is included at the top-left for comparison. Clockwise from the top-right: the $\gamma = 5/3$ run, the $\gamma = 4/3$ run and the $\gamma = 6/5$ run. All three projections are scaled to the correct relative size so interface locations can be directly compared. Image of Tycho taken from Warren et al. (2005).

- Pure 3D hydro
  - effects of particle acceleration
    - effective gamma

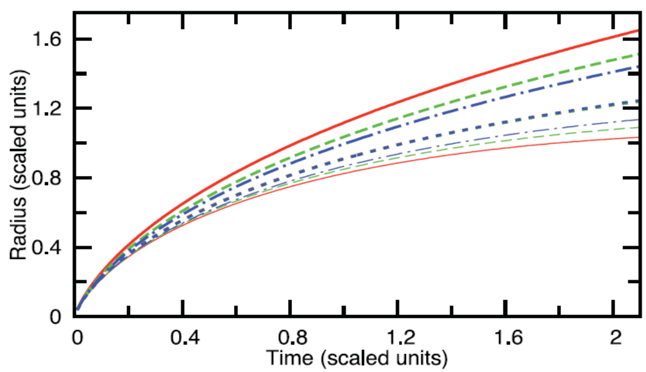

Figure 2. Interface locations as a function of time and adiabatic index for the exponential model in one dimension. The forward shock is tracked by thick lines, the reverse shock by thin lines, and the contact discontinuity by dotted lines. The curves for $\gamma = 5/3$, $\gamma = 4/3$ and $\gamma = 6/5$ are in red (solid), green (dashed) and blue (dash-dotted) respectively. The three curves for the contact discontinuity are separated by less than the width of the line used to show them.

3D MHD simulation : Role of ejecta clumping

- Small separation between the FS and CD (SN1006 : Miceli et al. 2009) can be explain by ejecta clumping

Orlando et al. 2011

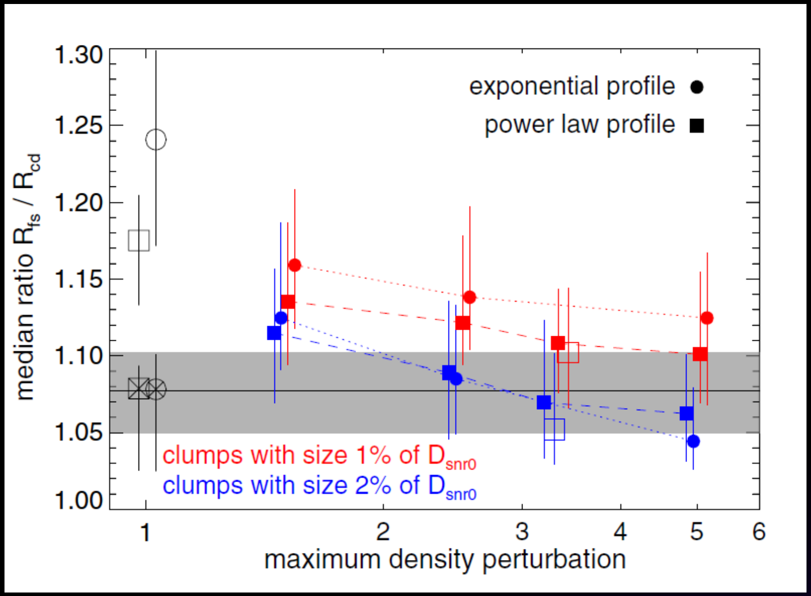

- 3D MHD
- effective gamma depends on oblique angle (quasi-parallel)

$$\gamma_{\rm eff} = \gamma - (\gamma - \gamma_{\rm min}) \times f_{\varsigma}(\Theta_{\rm o}),$$

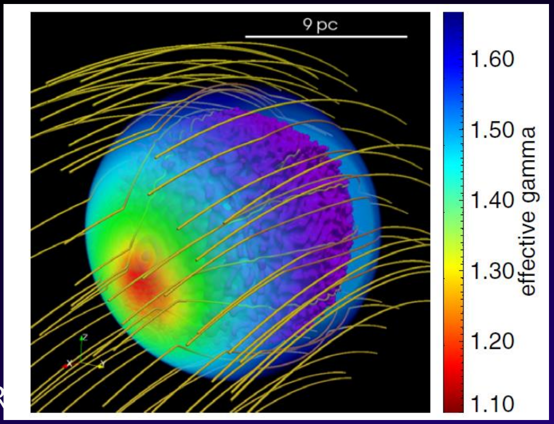

3D simulation of the thermal X-ray emission from young SNRs including efficient particle acceleration

Ferrand et al. 2012

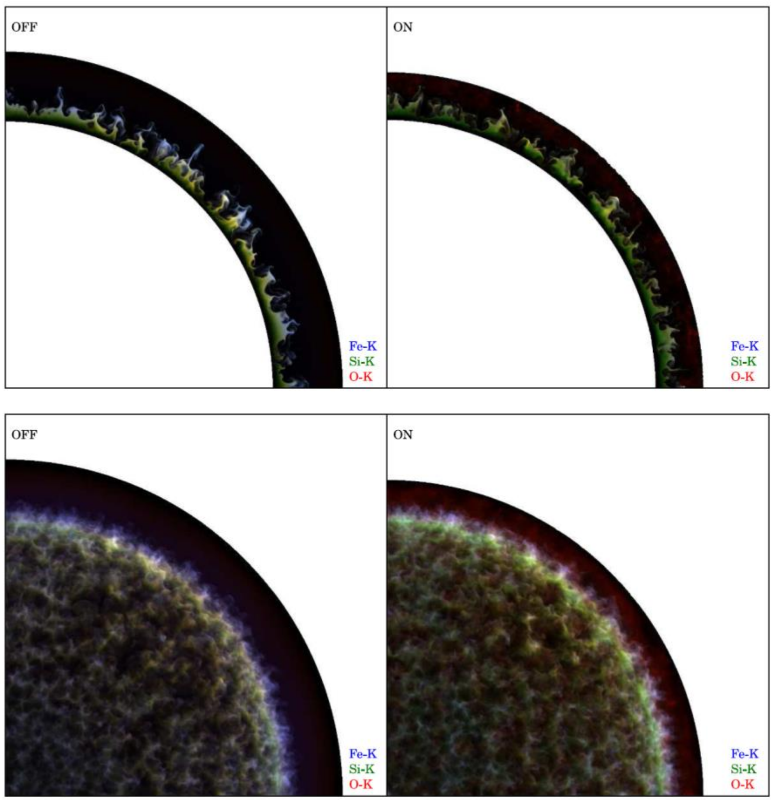

Figure 12. RGB rendering of three line emissions. For each pixel, the value of the red/green/blue channel is assigned from the emissivity of, respectively, the O–K band/Si–K band/Fe–K band, as displayed in Figures 8–10 (linearly normalized to 256 levels). Regions of pure blue, for instance, are dominated by Fe–K line emission. Regions of yellow = red + green are made out of a blend of O–K and Si–K line emission. Top: slices in the $z = 0$ plane; bottom: projected maps along the z-axis. Cases without ("OFF," on the left) and with ("ON," on the right) back-reaction of particles are compared.

(A color version of this figure is available in the online journal.)

- 3D simulation
- Diffusive Shock Acceleration
- Back reaction from accelerated particle
- Non-equilibrium ionization
- Thermal X-ray emission

Ferrand et al. 2014
Non-thermal broad-band emission

ASTRO-H

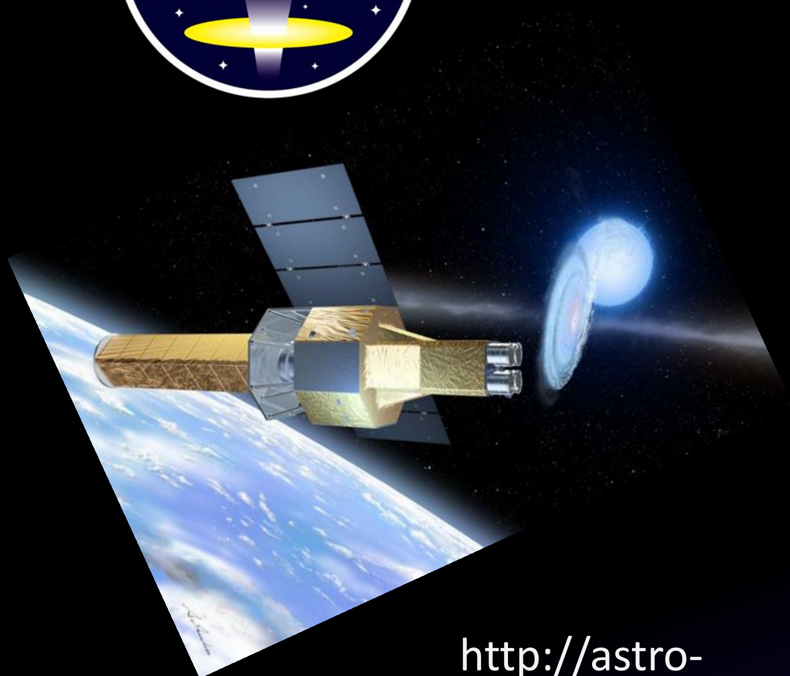

http://astro-h.isas.jaxa.jp/gallery/satelite/02.html

- New exploration X-ray Telescope
  - First right will be 2015 yr
  - 10 times larger energy resolution

High resolution spectrum of X-ray from SNRs is expected

Multi-D hydrodynamic simulation

- 1, 2D (3D in near future) hydro. with FLASH code
- Advection of elements
- Non-equilibrium ionization (NEI)
  - H, He, C, N, Ne, Mg, Si, S, Ar, Ca, Fe, Ni
- Different thermal energies between electrons and ions
- Heating of electrons due to Coulomb interaction
- Initial ejecta density : a power law profile

Radial profiles of temp., ionization

50% of ions are singly ionized (except for hydrogen)

beta = $T_e/T_{ion} = m_e/m_{ion}$

$$\frac{1}{2}m_{\rm i}v_{\rm sh}^2 \sim \frac{3}{2}k_{\rm B}T_{\rm i} \qquad \frac{1}{2}m_{\rm e}v_{\rm sh}^2 \sim \frac{3}{2}k_{\rm B}T_{\rm e}$$

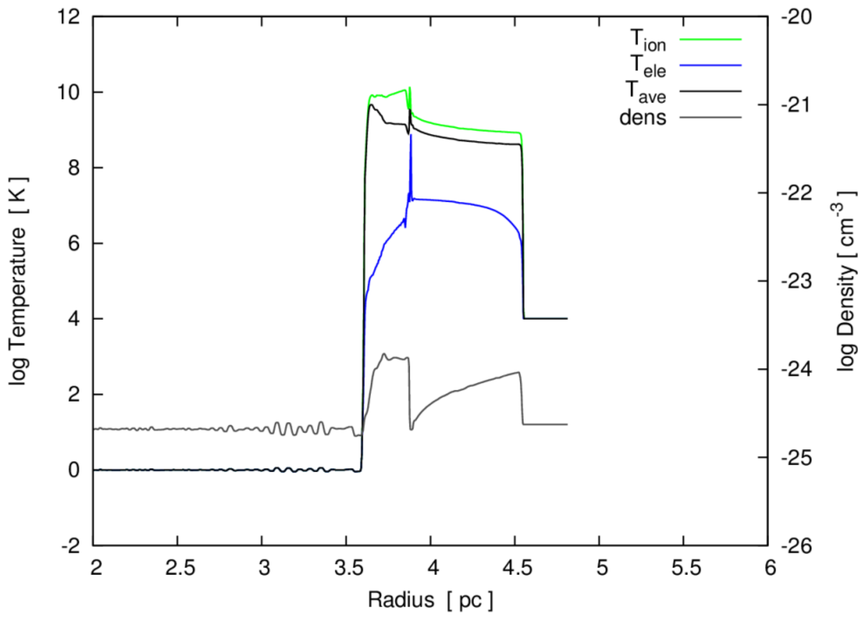

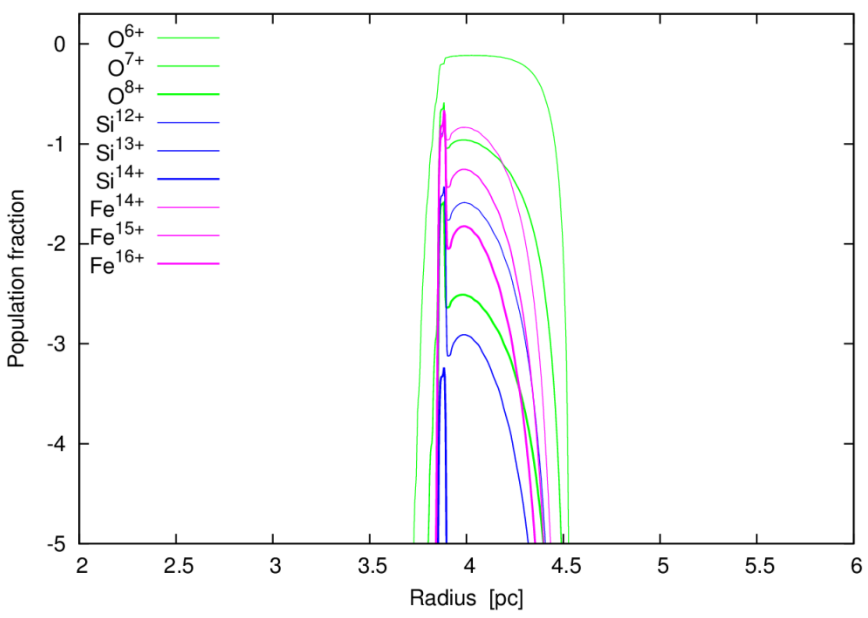

Efficient collisionless heating of electrons at RS

Yamaguchi et al. 2014 (X-ray observations of Tycho by SUZAKU)

beta = T_e/T_{ion}

- If beta = m_e/m_{ion}, beta ~ 10^{-5}
- beta = 0.01 is required for Tycho
- Possible mechanism
  - Cross-shock potential

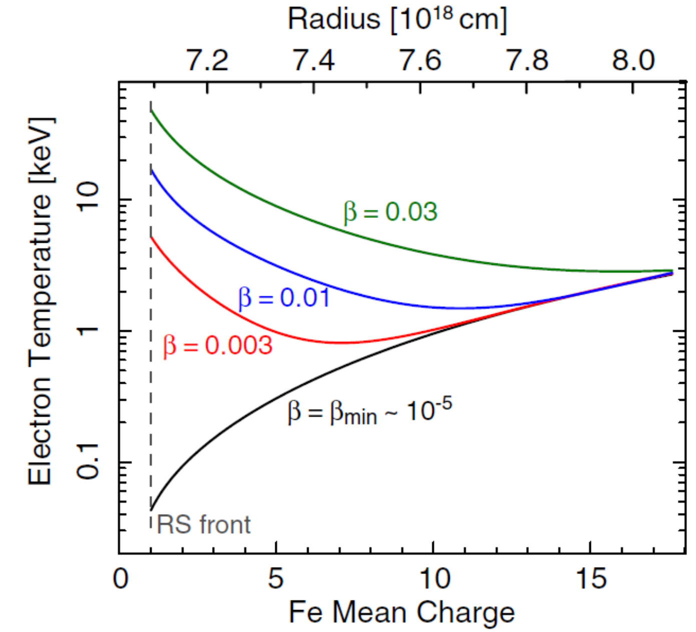

Figure 7. Electron temperature as a function of the mean charge of Fe ions from our hydrodynamical simulations. The corresponding radius is also given above. The black curve is the β_{min} model where no collisionless electron heating is assumed. The temperature ratio between the electrons and ions at the RS front is, therefore, set by their mass ratio. The models represented by the red, blue, and green curves assume that collisionless electron heating occurs at the RS, parameterized by ($\beta = T_e/T_{ion}$) with values set to 0.003, 0.01, and 0.03, respectively.

Radial profiles of temp., ionization

50% of ions are singly ionized (except for hydrogen)
beta = $T_e/T_{ion} = m_e/m_{ion}$ x 1e2

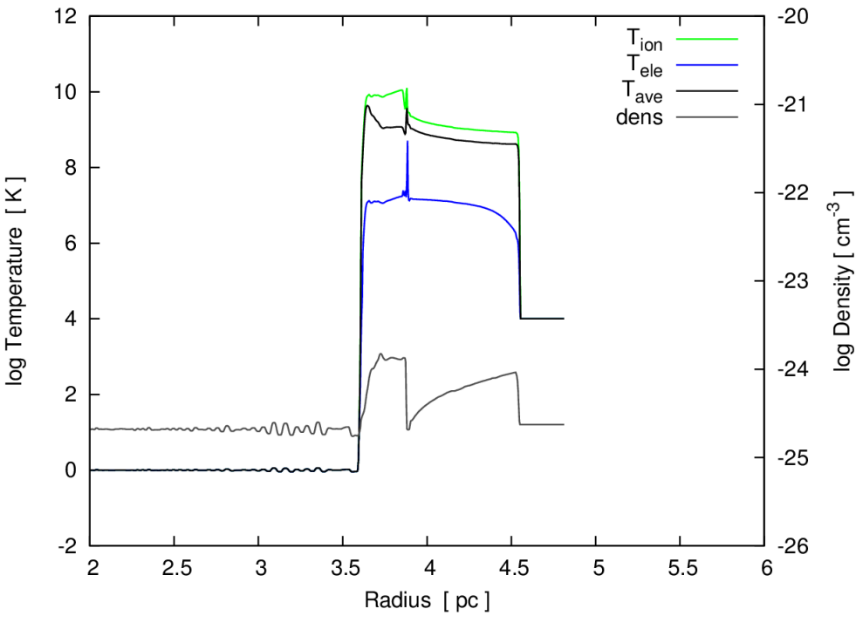

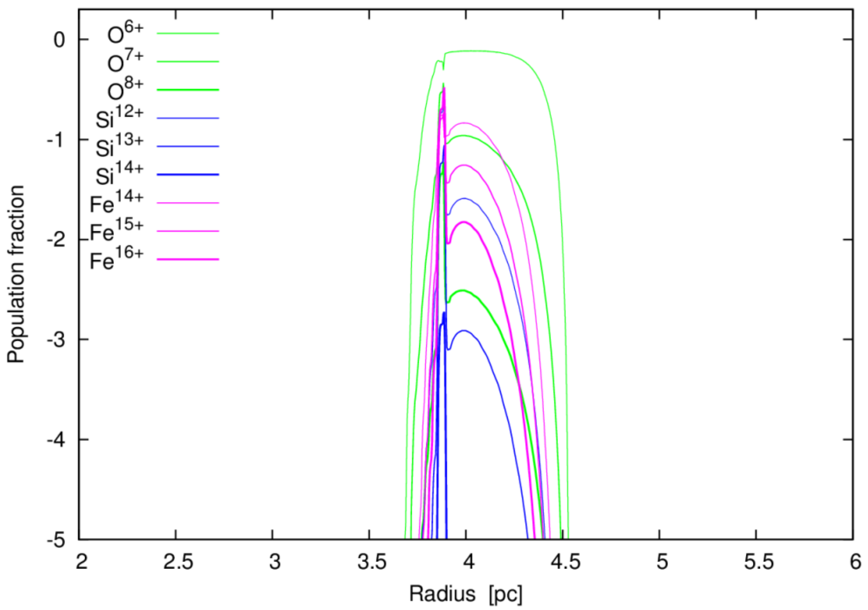

Density

Ejecta density profile : Power-law of n=7 with inner flat regions
Non-Uniform ejecta Comp. : W7

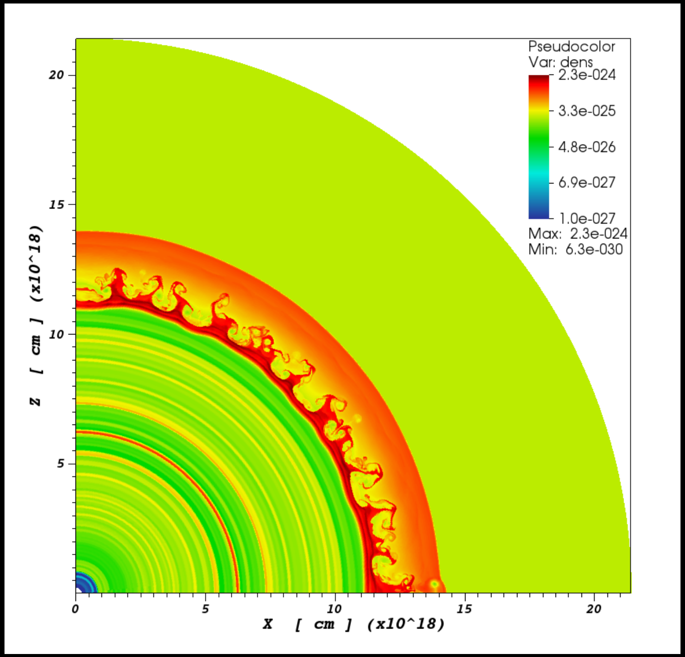

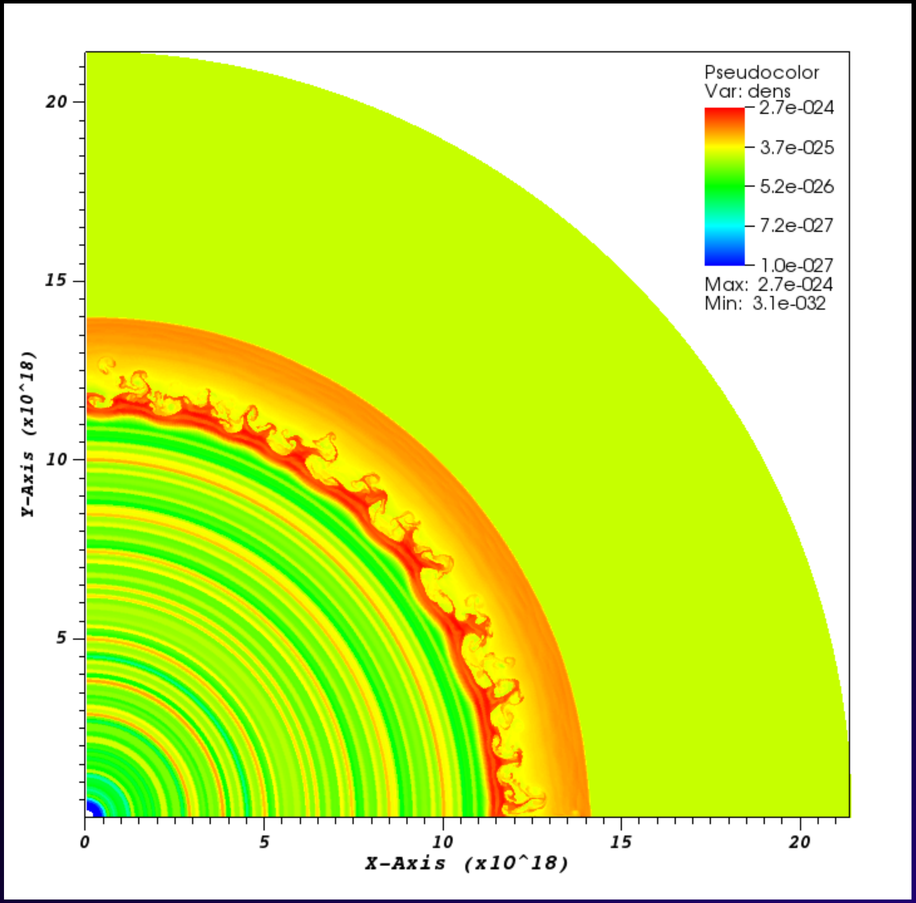

Uniform ejecta Comp. :
Offset-DDT model
(Maeda et al. 2010)

Electron temperature

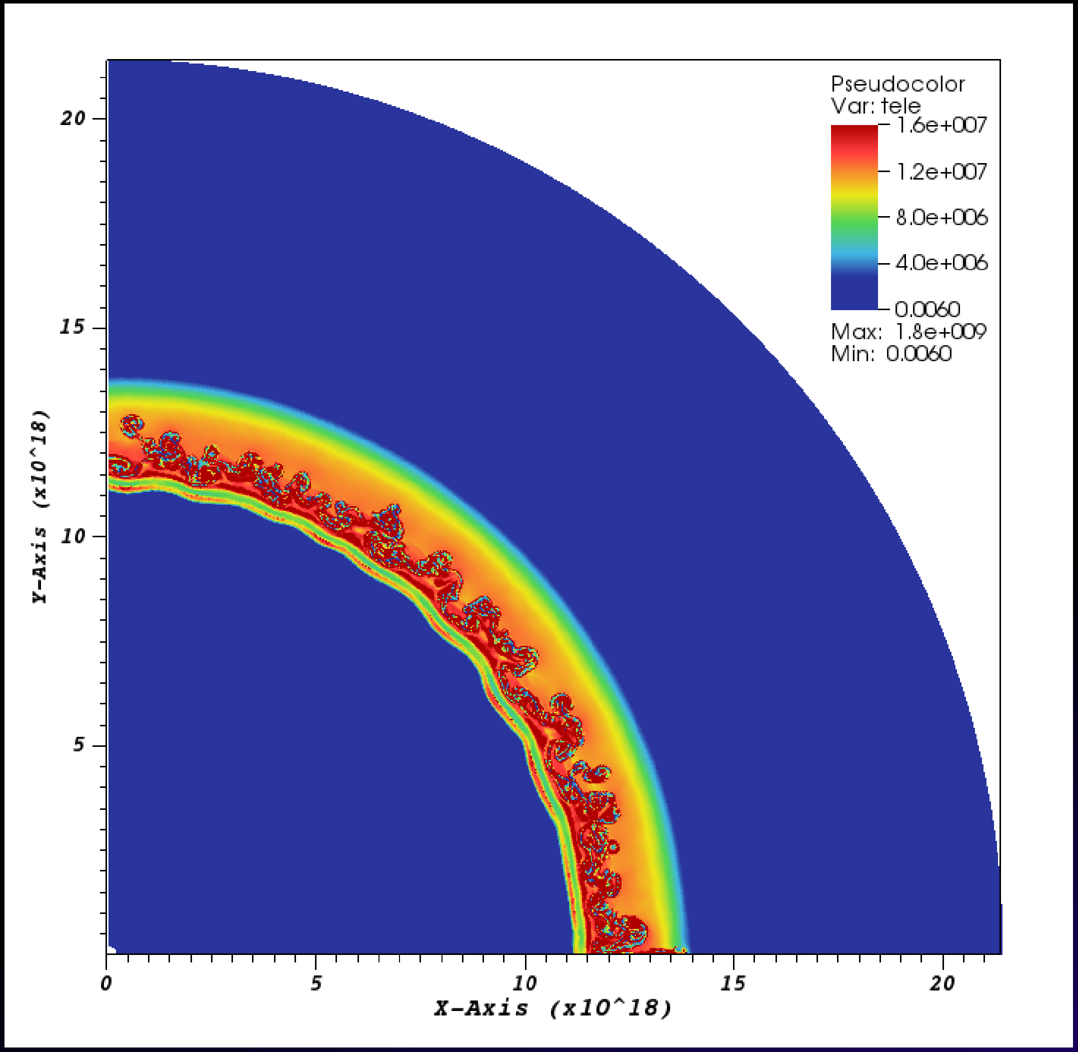

Distribution of elements

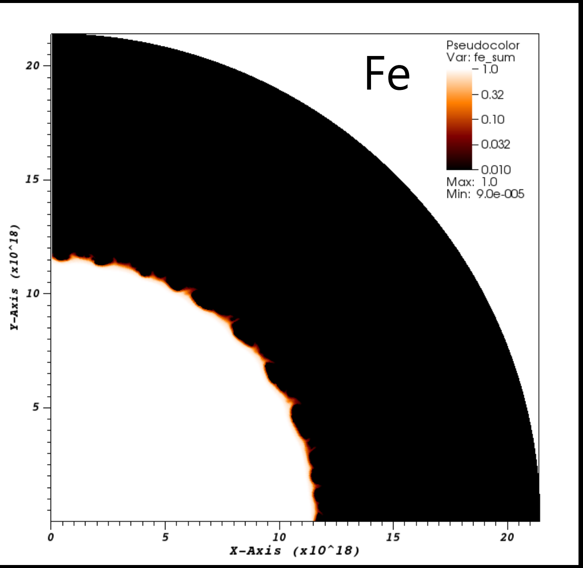

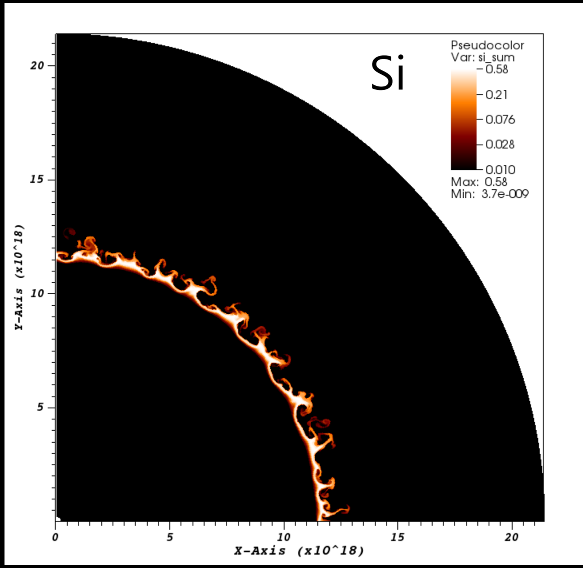

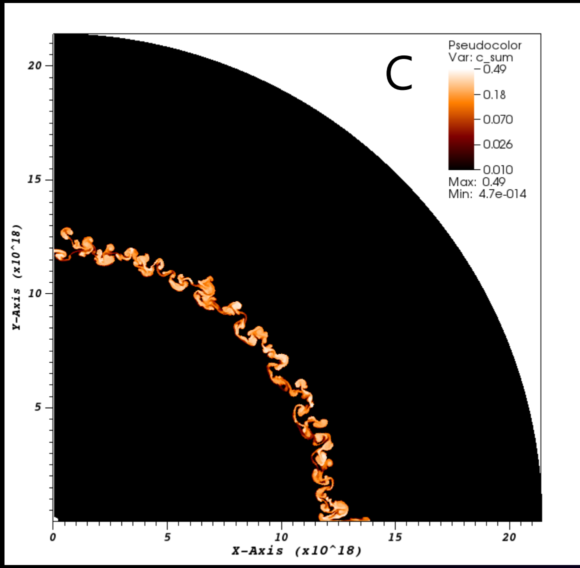

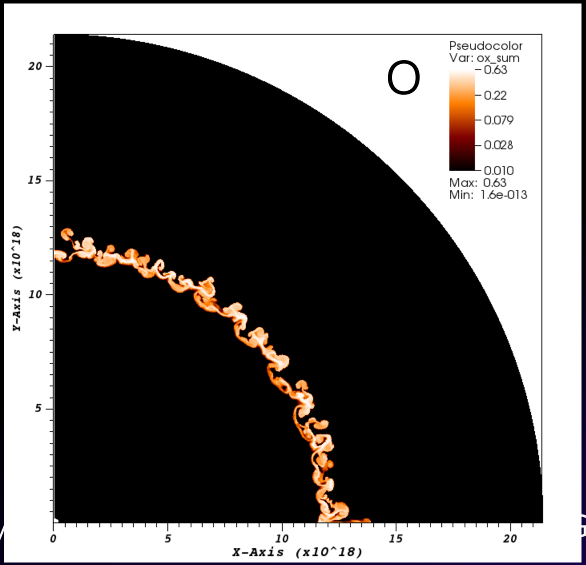

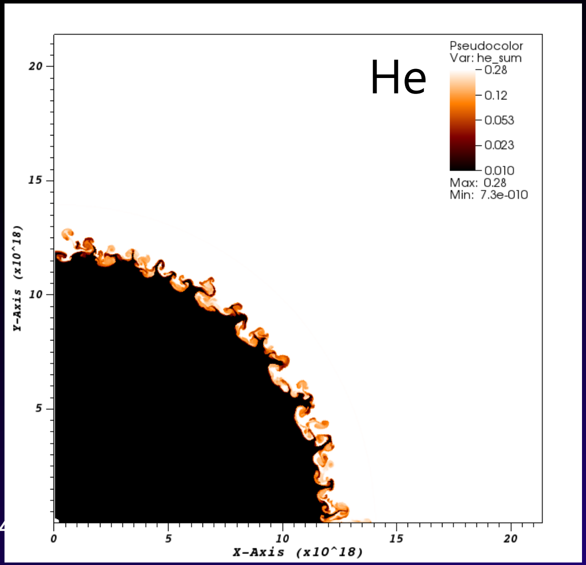

Spectrum (continuum + thermal X-ray)

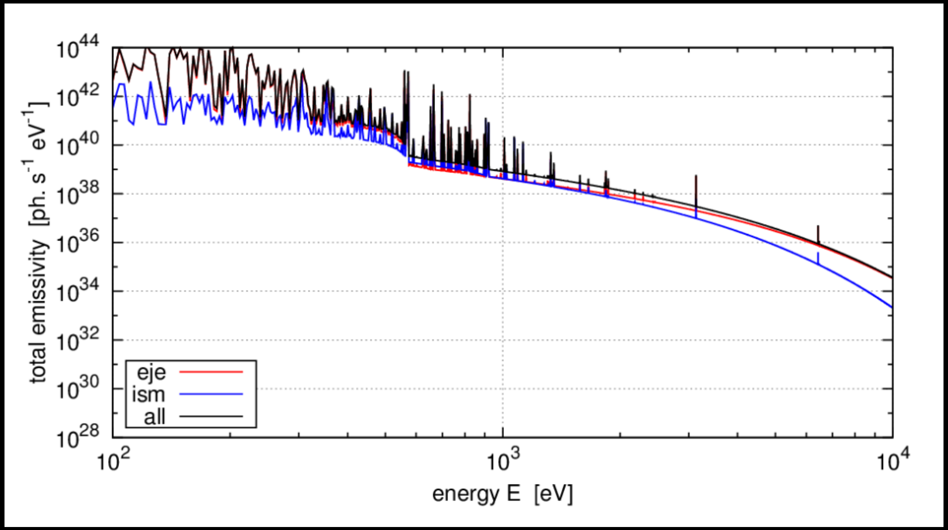

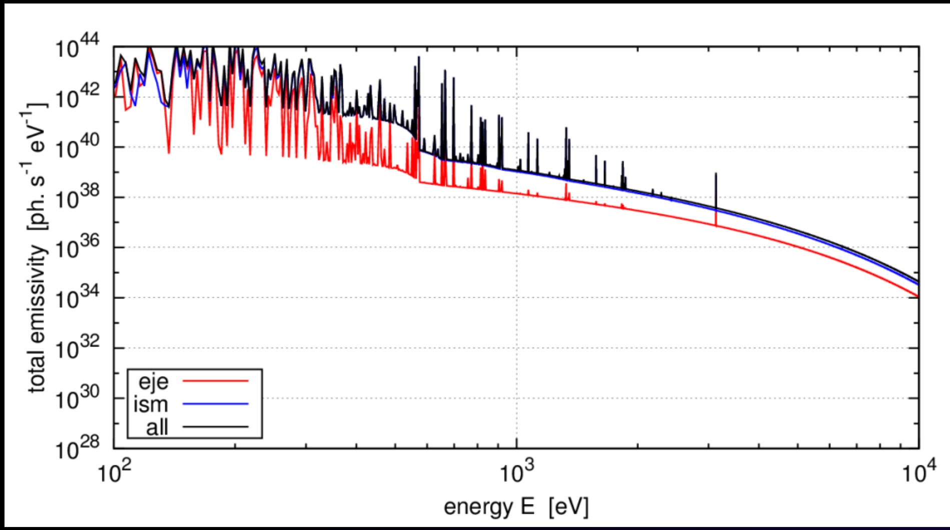

Uniform ejecta Comp. :
Offset-DDT model
(Maeda et al. 2010)

Non-Uniform ejecta Comp. :
W7 (Nomoto et al. 1984)

3D MHD simulation

- 3D MHD simulation. with FLASH code
- An unsplit MHD solver
- Constraint transport (CT) method for div B = 0

Initial clumpy ejecta for a Type Ia SN

Exponential ejecta profile for Type Ia SNRs
Dwarkadas & Chevalier 1998

$$\rho_{\rm SN} = A \exp(-v/v_{\rm ej})\, t^{-3}$$

$$v_{\rm ej} = \left(\frac{E_{\rm kin}}{6\, M_{\rm ej}}\right)^{1/2} \quad v = r/t$$

$$A = \frac{6^{3/2}}{8\,\pi}\,\frac{M_{\rm ej}^{5/2}}{E^{3/2}}$$

$$P = \kappa\,\rho^{4/3}$$ Wang 2005

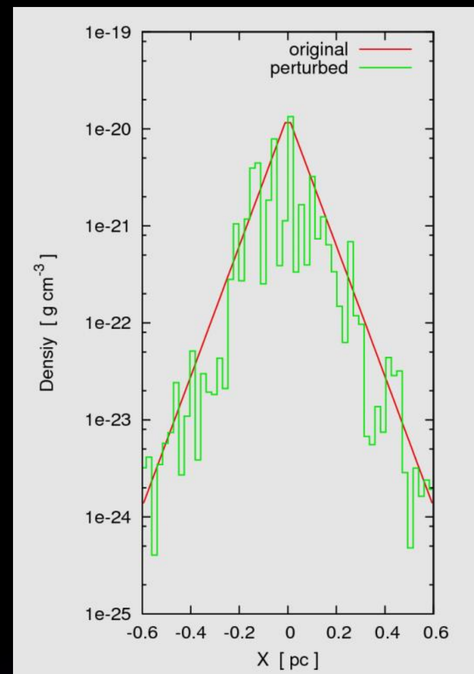

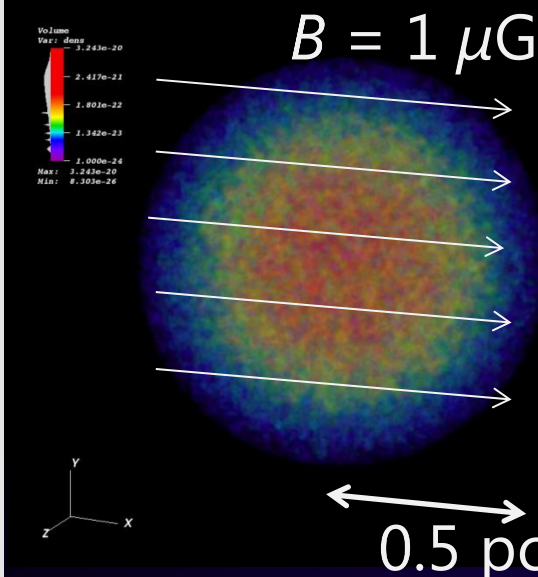

$E_{\rm kin}$: kinetic energy (10^{51} erg)
$M_{\rm ej}$: ejecta mass (1.37 $M_\odot$)

Volume rendering images of density

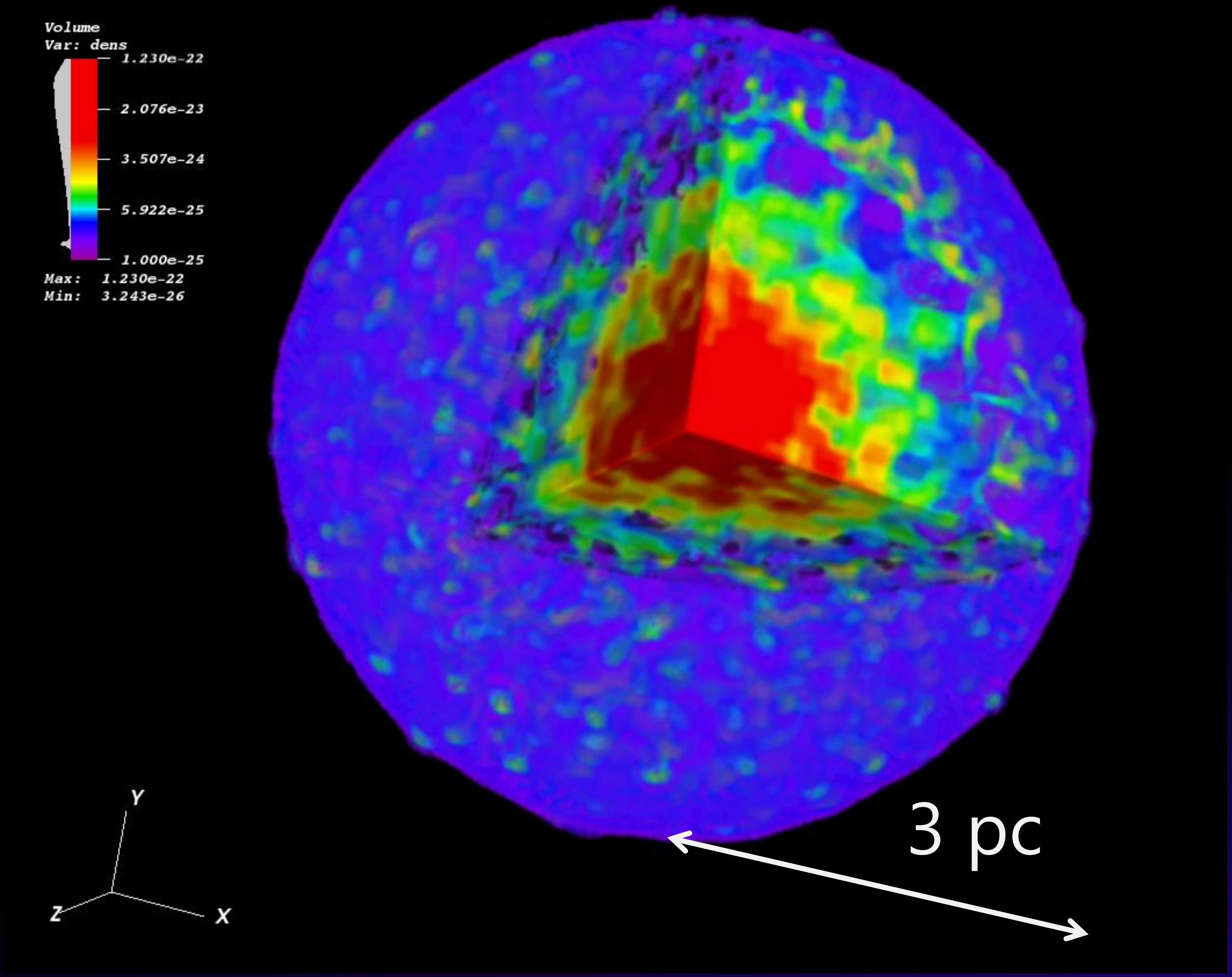

Amplified magnetic field

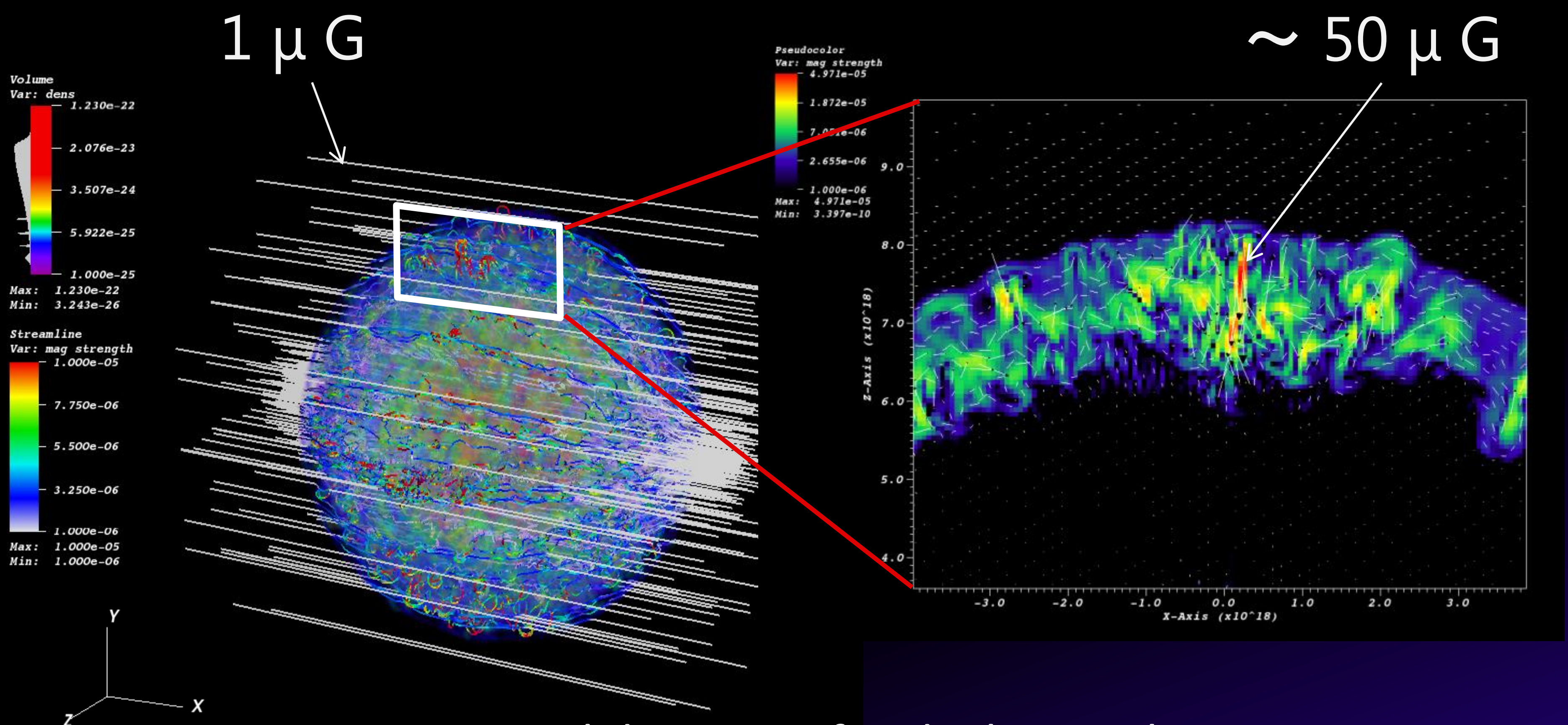

Computational domain is fixed. The resolution is dominated by the maximum refinement level

3D MHD simulation of a SNR with remapping

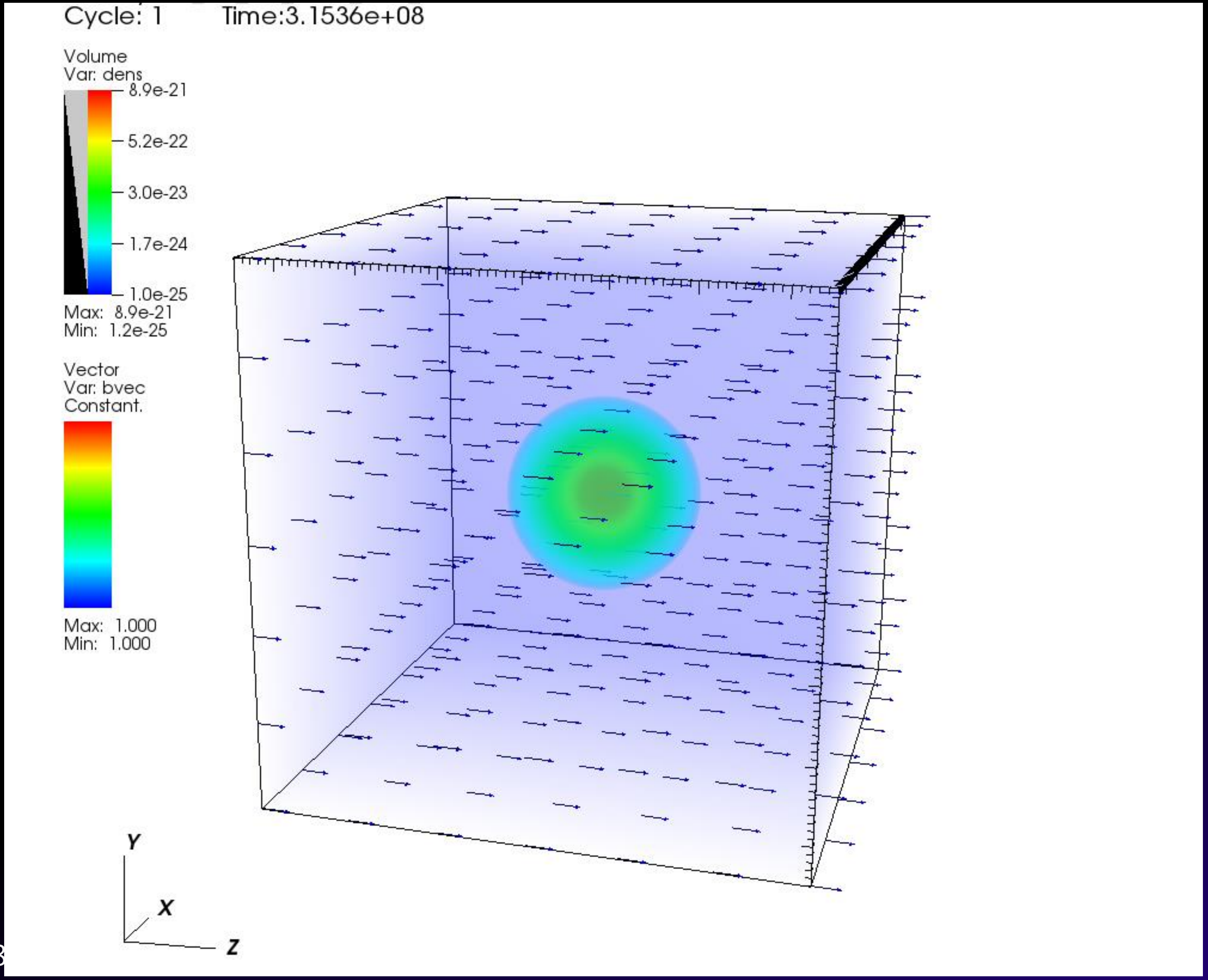

Density

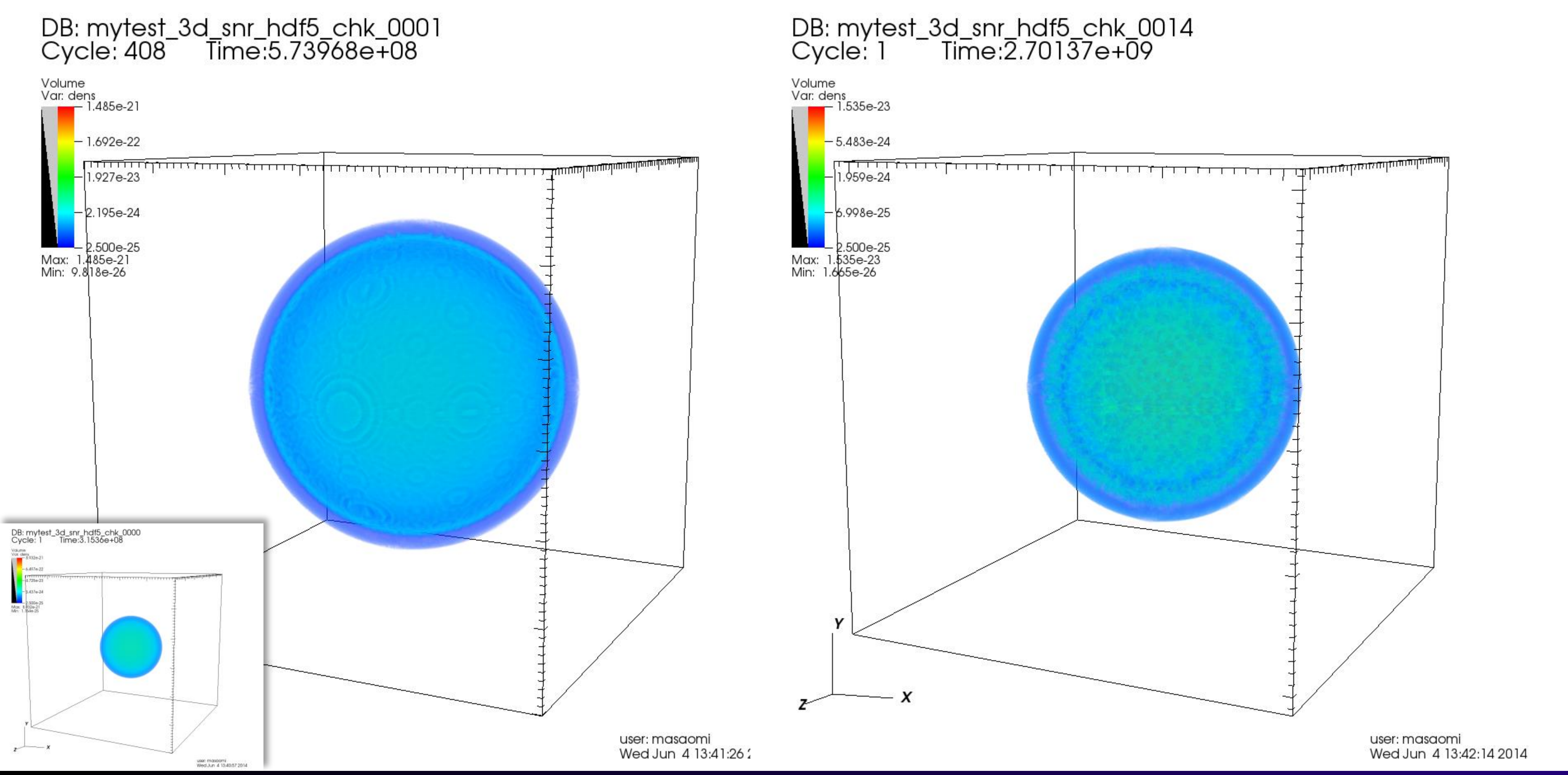

DB: mytest_3d_snr_hdf5_chk_0001
Cycle: 408 Time:5.73968e+08
Volume
Var: dens
1.485e-21
1.692e-22
1.927e-23
2.195e-24
2.500e-25
Max: 1.485e-21
Min: 9.818e-26
user: masaomi
Wed Jun 4 13:41:26
DB: mytest_3d_snr_hdf5_chk_0000
Cycle: 1 Time:3.1536e+08
DB: mytest_3d_snr_hdf5_chk_0014
Cycle: 1 Time:2.70137e+09
Volume
Var: dens
1.535e-23
5.483e-24
1.959e-24
6.998e-25
2.500e-25
Max: 1.535e-23
Min: 1.665e-26
Y
Z
X
user: masaomi
Wed Jun 4 13:42:14 2014

CT (Constraint Transport) method : magnitude of the B-field

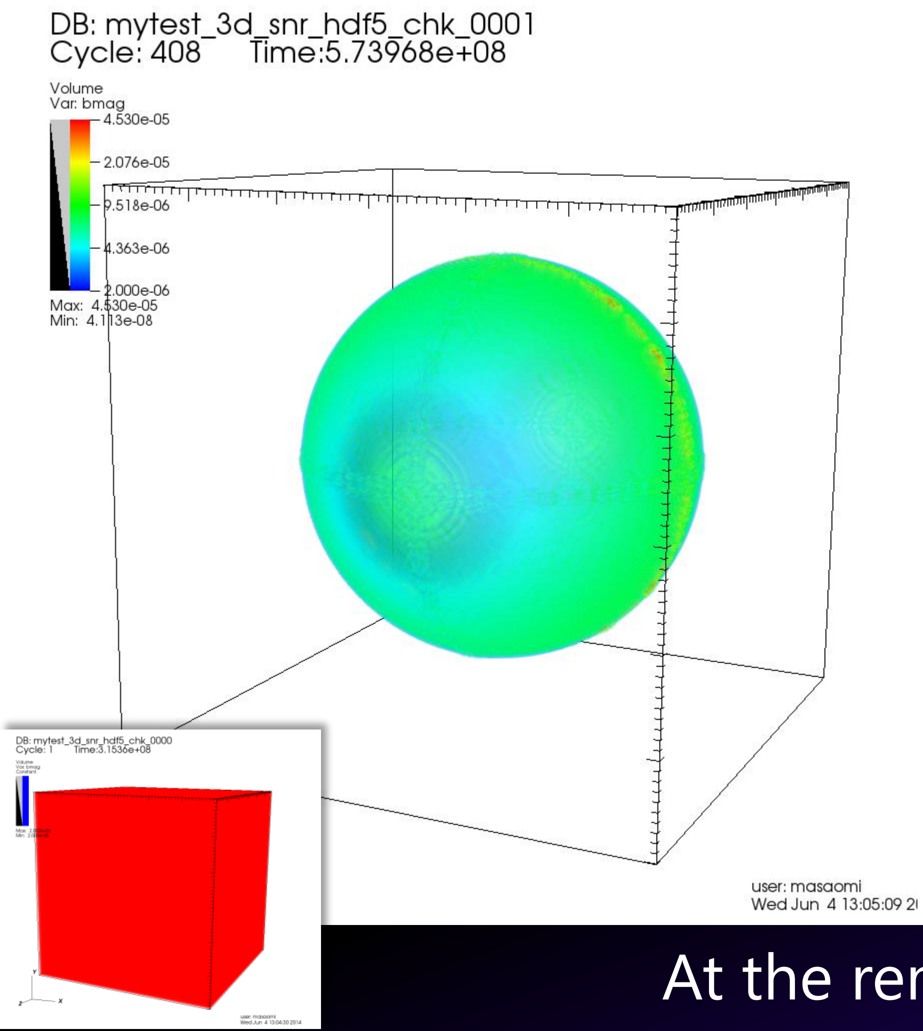

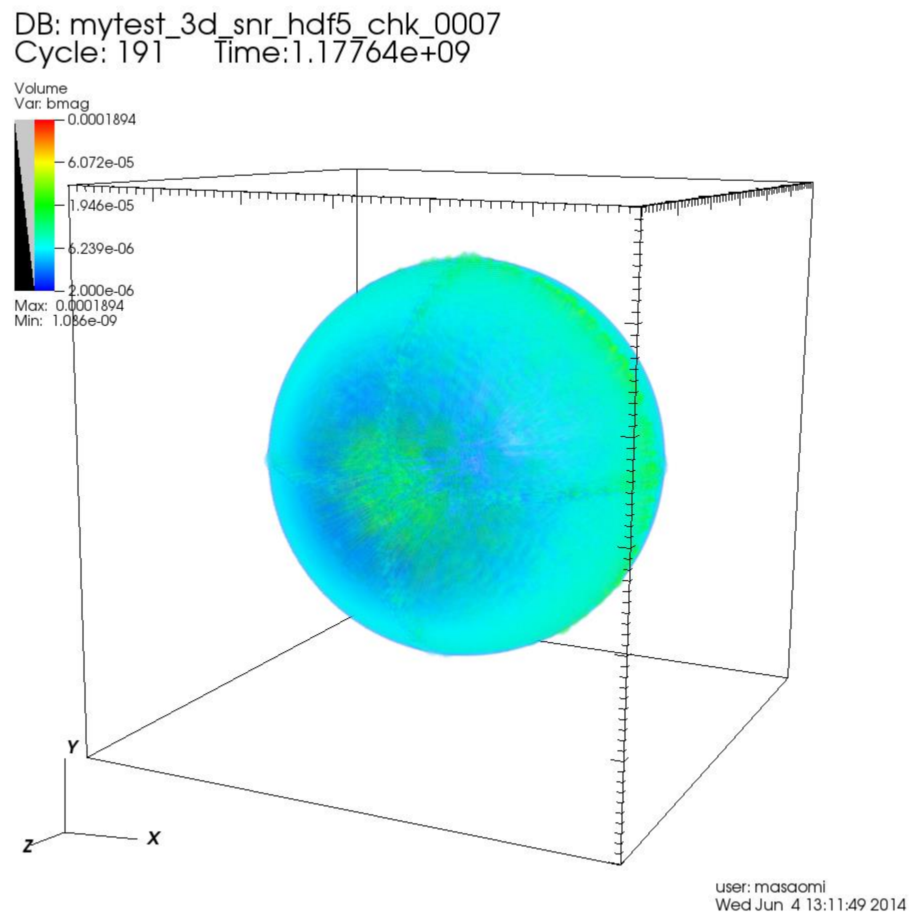

At the remapping, div B = 0 is broken

Summary

- Multi-D theoretical models of SNRs
- Test multi-dimensional simulations
  - 1, 2-D hydrodynamic simulation
  - 3-D MHD simulation
- Still the code developments are under going
- In (near?) future,
  - Realistic explosion model, Multi-D (M)HD simulation with a NLDSA